ADVANCED ENERGY MATERIALS
www.advenergymat.de

Polyacrylic Acid Assisted Assembly of Oxide Particles and Carbon Nanotubes for High-Performance Flexible Battery Anodes

Yanhua Cheng, Zheng Chen, Meifang Zhu, and Yunfeng Lu**

Oxides of transition metal hold great potential as high-capacity anode materials for lithium-ion batteries. Implication of such materials for large-scale applications, however, has been limited by their low ionic and electronic conductivity, as well as poor cycling stability.[1] To improve the electronic conductivity, carbons are commonly used as conductive agents, either by directly mixing with oxide particles or by forming carbon–oxide composites. To improve the ion transport, using oxides with low-dimensional structure (e.g., nanoparticles[2] and nanowires[3]) with shortened ion diffusion length has been a common strategy. To improve the stability, approaches such as using electrolyte additives, controlling electrode composition and structure were explored extensively.[4,5] Among these efforts, building nanocomposite architecture with nanocarbon and oxide nanoparticles is of great interest, because of the synergic effects resulted from the shortened ionic diffusion length and enhanced electronic conductivity. Furthermore, through engineering the interface between the carbon and the oxide nanoparticles, it is possible to develop highly robust nanocomposites with greatly improved storage performance.[6,7]

To date, nanocomposites of carbon and oxide nanoparticles are generally synthesized by depositing oxides on carbon scaffolds using sol–gel coating,[8] chemical vapor deposition (CVD),[9,10] solution growth,[11,12] self-assembly,[13,14] or other methods.[15] The assembly approach, which generally utilizes hydrophobic interactions between a carbon scaffold (e.g., carbon nanotubes (CNTs)) and oxide nanoparticles stabilized by hydrophobic ligands,[16] enables the formation of various nanocomposites with good energy storage capability. However, making hydrophobic nanoparticles requires extensive use of capping agents, and the synthesis process is often complicated. On the other hand, a large variety of oxide nanoparticles can be readily synthesized with hydrophilic surface at large scale. Therefore, it is of great interest to develop a general approach that can enable the assembly of hydrophilic nanoparticles with a carbon scaffold.

CNTs have been used in electrode materials as the conductive additive with metal oxides for flexible batteries applications, since they exhibit high aspect ratio, excellent conductivity, and good mechanical properties. However, to make flexible electrodes, an electrochemically inert substrate (e.g., plastic) is often used to provide enough mechanical strength. For example, flexible alkaline batteries by implementing multiwalled CNTs and copolymer separator using polyethylene terephthalate film as substrate was demonstrated.[17] Most of prior works on freestanding electrodes have been based on in situ growth or deposition of oxide thin films on more costly super-long CNTs or super-aligned CNT arrays which show better mechanical properties. For example, super-long CNTs enabled fabrication of freestanding flexible CNT/V_2O_5 electrodes with robust structure.[18] CNTs/Fe_3O_4 flexible anodes have been realized by magnetron-sputtered deposition of Fe_3O_4 nanoparticles onto aligned CNT scaffolds that were drawn from CNT arrays.[19]

It has been known that some polymers (e.g., poly(acrylic acid), PAA) can be effectively wrapped around CNTs,[20] forming CNTs/polymer composites with conductivity comparable to that of the pristine CNTs.[21] In addition, hydrophilic oxide nanoparticles with a large number of hydroxyl (–OH) groups on outer surfaces[22] can also interact strongly with polymer such as PAA through hydrogen or electrostatic bonding.[23,24] As depicted in **Figure 1**A, utilizing the interactions of PAA with both the nanoparticles and the CNTs, it is possible to assemble such hydrophilic nanoparticles around the CNTs scaffolds into nanocomposites; filtration process leads to the formation of a freestanding flexible nanocomposite film; subsequent heat treatment further strengthens the networks of the nanoparticles forming robust composite spheres threaded by the CNTs.

To demonstrate the concept of the polymer-assisted assembly, hydrophilic nanocrystals (NCs) of iron oxide (Fe_3O_4) produced by aqueous solution growth were used as the active material owning to the high-energy capacity, low cost, and low toxicity.[25] The –OH groups on the surfaces of Fe_3O_4 particles were characterized by Fourier transform infrared (FTIR) spectroscopy (Figure S1, Supporting Information), which shows the adsorption in the range of 3000–3600 cm^{-1}.[22] Experimentally, PAA was first added to dimethyl sulfoxide (DMSO) containing CNTs; then NCs dispersed in ethanol (Figure 1B) were added into the mixture resulting in the formation of CNTs/NCs assemblies that were precipitated from the suspension (Figure 1C). A following filtration process afforded the formation of composite films; further annealing process crosslinks the polymer, NCs

Dr. Y. Cheng, Prof. M. Zhu
State Key Laboratory for Modification
of Chemical Fibers and Polymer Materials
College of Materials Science and Engineering
Donghua University
Shanghai 201620, P. R. China
E-mail: zmf@dhu.edu.cn
Dr. Y. Cheng, Dr. Z. Chen, Prof. Y. Lu
Department of Chemical and Biomolecular Engineering
University of California
Los Angeles, CA 90095, USA
E-mail: luucla@ucla.edu

DOI: 10.1002/aenm.201401207

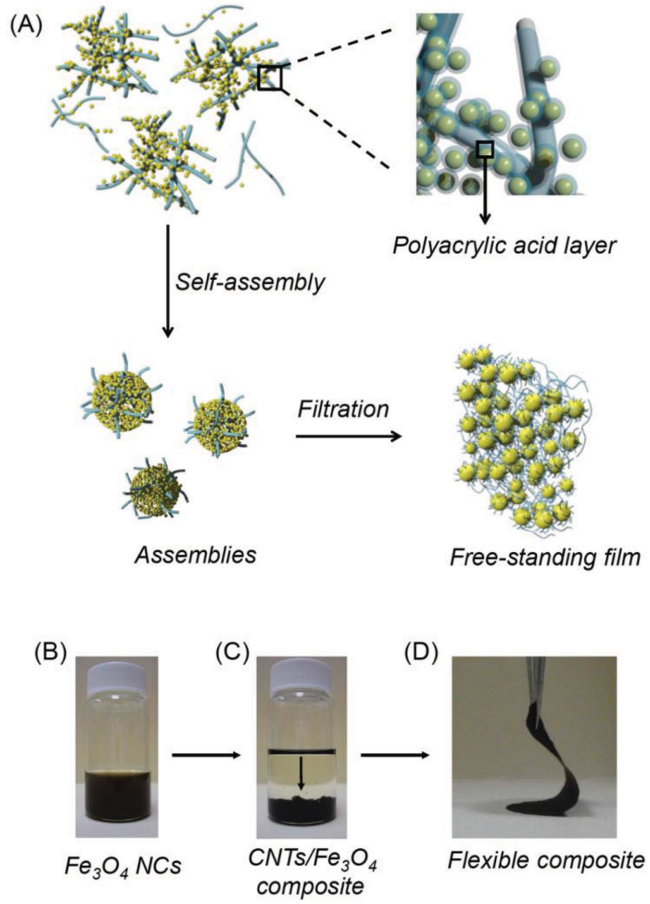

Figure 1. A) Schematic illustration of the fabrication of flexible CNTs/NCs composite electrodes through polymer-assisted assembly and the digital graphs of, B) Fe_3O_4 NCs suspension, C) assembled structure of $CNTs/Fe_3O_4$, and D) flexible electrode made using a filtration technique.

and the CNTs, constructing robust and flexible thin film electrodes (Figure 1D).

In this study, PAA plays an important role in serving as a multifunctional agent to provide good mechanical and electrochemical properties. The carboxylic groups (–COOH) that bind CNTs networks and active materials together through the interaction between carboxylic (–COOH) groups in PAA and hydroxyl (–OH) groups on the surfaces of active materials provides good mechanical integrity of the electrodes.[26] The dynamic hydrogen bonds between PAA and active materials were proposed to exhibit a self-healing effect that allows reforming electronic conduction pathway if local composite structure is broken.[26] Moreover, PAA can also provide electrostatic interaction between carboxylic groups and Li-ions for good ion conductivity[27] and prevent the undesired swelling of the electrodes in the organic electrolyte.[28] After annealing the electrodes, the polymeric layers on CNTs and active materials form the cross-linked network to further prevent the anode from disintegration.[29] In such composite architecture, the NCs provide energy storage materials with shortened Li-ion diffusion length, while the CNTs threaded through the NCs clusters offer continuous electron conductive pathways. These favorable features afford the composites with high performance storage capability and cycling stability.

The synthesized Fe_3O_4 NCs possess a face-centered-cubic structure as indicated by the X-ray diffraction (XRD) pattern (Figure S2, Supporting Information). **Figure 2**A shows a transmission electron microscopic (TEM) image of the NCs, indicating a uniform size with an average diameter of ≈10 nm. Thermal gravimetric analysis (TGA) shows that the $CNTs/Fe_3O_4$ composites are composed of ≈70 wt% Fe_3O_4 (Figure S3, Supporting Information). Figure 2B presents a scanning electron microscopic (SEM) image of the resulted composite, clearly revealing a network structure that is made from the assembled NCs and the threading CNTs, which is further confirmed by the TEM image shown in Figure 2C. Note that PAA and weakly oxidized CNTs contain a large number of carboxylic groups (–COOH); during the heat treatment of the composites, such groups may self-react forming anhydride bonds or react with the hydroxyl (–OH) groups on NCs forming ester bonds. Consistently, FTIR of the composites exhibit the characteristic stretching for the anhydride and ester bonds at 1801 and 1720 cm^{-1},[29] respectively (Figure S4, Supporting information). The formation of such bonds crosslinks the CNTs, PAA, and NCs into robust 3D network structure.

Figure 2D shows nitrogen adsorption and desorption isotherms of the composite. The composite exhibits a typical type IV isotherm with significant nitrogen uptake at relative pressure above 0.6 with a surface area of 109 m^2 g^{-1}. As shown in the inset of Figure 2D, based on the desorption isotherm and the Barrett–Joyner–Halenda (BJH) method, the composite exhibits a broad pore size distribution centered at 20 nm. Combining the macropores observed from the SEM and TEM studies (Figure 2B, C), it is reasonable to conclude that the composite contains a hierarchically porous structure with high surface area. Such hierarchical structure is of importance to ensure effective ion transport while provide abundant active sites. On the other hand, the sufficient internal porosity provides the space to buffer the mechanical stress and large volume changes.

Coin cells with metallic Li as the both counter and reference electrodes were employed to evaluate their electrochemical behavior. **Figure 3**A shows representative cyclic voltammetry (CV) curves for the electrode at sweep rate of 0.5 mV s^{-1} within a cutoff voltage window of 0.005–3.0 V. In the first cathodic sweep, three peaks are observed at 1.5, 0.8, and 0.6 V, which are attributed to the structural transition from crystalline Fe_3O_4 to $Li_xFe_3O_4$, the formation of solid electrolyte interface (SEI) layer and phase transition from $Li_xFe_3O_4$ to $Li_2Fe_3O_4$ and further reduction to Fe(0), respectively.[30,31] The broad peak at 1.8 V in the anodic process corresponds to the oxidation of Fe(0) to Fe(II) and Fe(III). In the subsequent curves, they show good reproducibility with a pair of cathodic and anodic peaks at around 0.7 and 1.8 V for the reversible redox reaction. The initial peaks at 1.5 and 0.8 V disappear as a result of irreversible structure change of Fe_3O_4 after full lithiation. The positive shift for cathodic peak to 0.7 V can be due to decreased polarization of the electrode materials from the first cycle.[32]

Figure 3B shows the galvanostatic charge/discharge curves of the electrode with a current density of 100 mA g^{-1} at the voltage window from 0.005 to 3 V. In the first charge curve, an extended plateau appears at approximately 0.8 V versus Li/Li^+, which is in good agreement with the CV profile and similar to

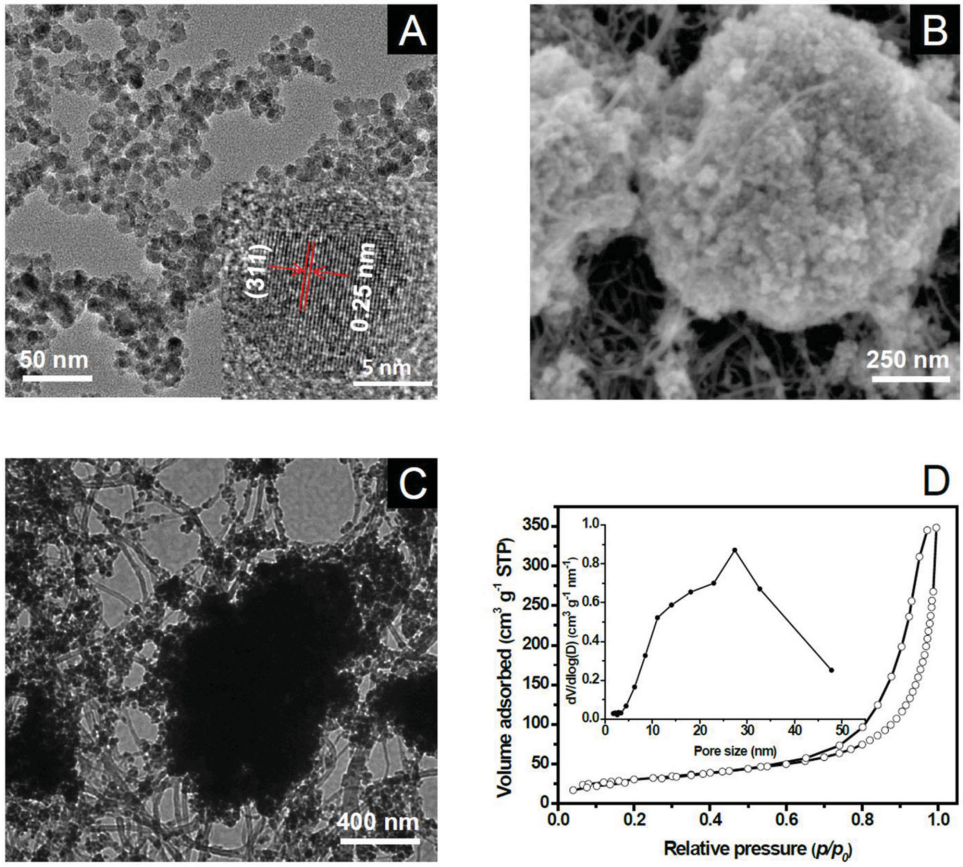

Figure 2. A) TEM and HRTEM (inset) image of Fe_3O_4 NCs, HRTEM image showing 311 (0.25 nm) lattice. B) SEM image of a CNTs/Fe_3O_4 electrode with spherical assemblies. C) TEM image of CNTs/Fe_3O_4 composites. D) Nitrogen adsorption isotherms of CNTs/Fe_3O_4 composites and pore-size distribution (inset) plot calculated by the BJH formula with the desorption isotherm.

the literature results.[33,34] It is found that the initial charge and discharge capacities are 1918 and 837 mAh g^{-1}, respectively. The high irreversible capacity loss is due to electrolyte decomposition and SEI formation.[35,36] After the initial cycle, the discharge capacity of CNTs/Fe_3O_4 hierarchical structures keeps good retention in the following cycles with ≈850 mAh g^{-1}.

The cycling stability of the composite is displayed in Figure 3C. The composite electrodes show a stable cycling performance up to 100 cycles of charge/discharge at a current density of 100 mA g^{-1}. After first three conditioning cycles, the Coulombic efficiency increases to above 98%. It is interesting to note that the capacity of the electrode increased to 1110 mA h g^{-1} during cycling. The additional capacity may be attributed to the reversible growth of a polymeric gel-like film resulting from degradation of the electrolyte at low potential.[37] Besides the good cycling stability, the electrodes also show a good rate performance. Benefiting from the unique hierarchical structure and the presence of threaded CNTs in the composites, the CNTs/Fe_3O_4 composites exhibit excellent rate capability. Figure 3D displays the charge/discharge capacities of the electrodes at different rates. Discharge capacity of 865, 795, 729, 668, and 609 mA h g^{-1} are obtained at charge/discharge rates of 100, 250, 500, 750, and 1000 mA g^{-1}, respectively. Remarkably, the capacity can be still retained at 974 mA h g^{-1} when the rate returns to 100 mA g^{-1}.

The durable performance of the electrode can be ascribed to the cross-linked CNTs/PAA networks, which is effective in holding the Fe_3O_4 particles together and accommodating volume change of the particles, as well as maintaining the electrical and ionic conductivity. The structure and interfacial behavior of the composite electrodes during the cycling process are better understood by electrochemical impedance spectroscopy (EIS) measurement. Nyquist plots of the CNTs/Fe_3O_4 electrodes at different cycling status are shown in Figure 3E. It is found that the fresh electrode shows a relatively small semicircle (≈30 Ω) and an intercept at high-frequency range, which is associated with a combination of ohmic and charge-transfer resistance. There is a slight increase in semicircle diameter (≈42 Ω) after ten cycles, which may be associated with forming SEI layer. The charge-transfer resistance of the electrode is nearly constant during cycling after 60 cycles, indicating the charge transfer pathway was retained during the cycling process. The following sloping region after semicircle in the low-frequency region presents the diffusion resistance of the electrolyte ions into the electrode. Due to the SEI layer formation, the slope region decreases continuously at the low-frequency region after 60 cycles, indicating an increased diffusion resistance. However, the electrodes still retain high capacities after cycling at different current density, which indicates that the ion diffusion pathways in the composites are not affected by the SEI formation.[38]

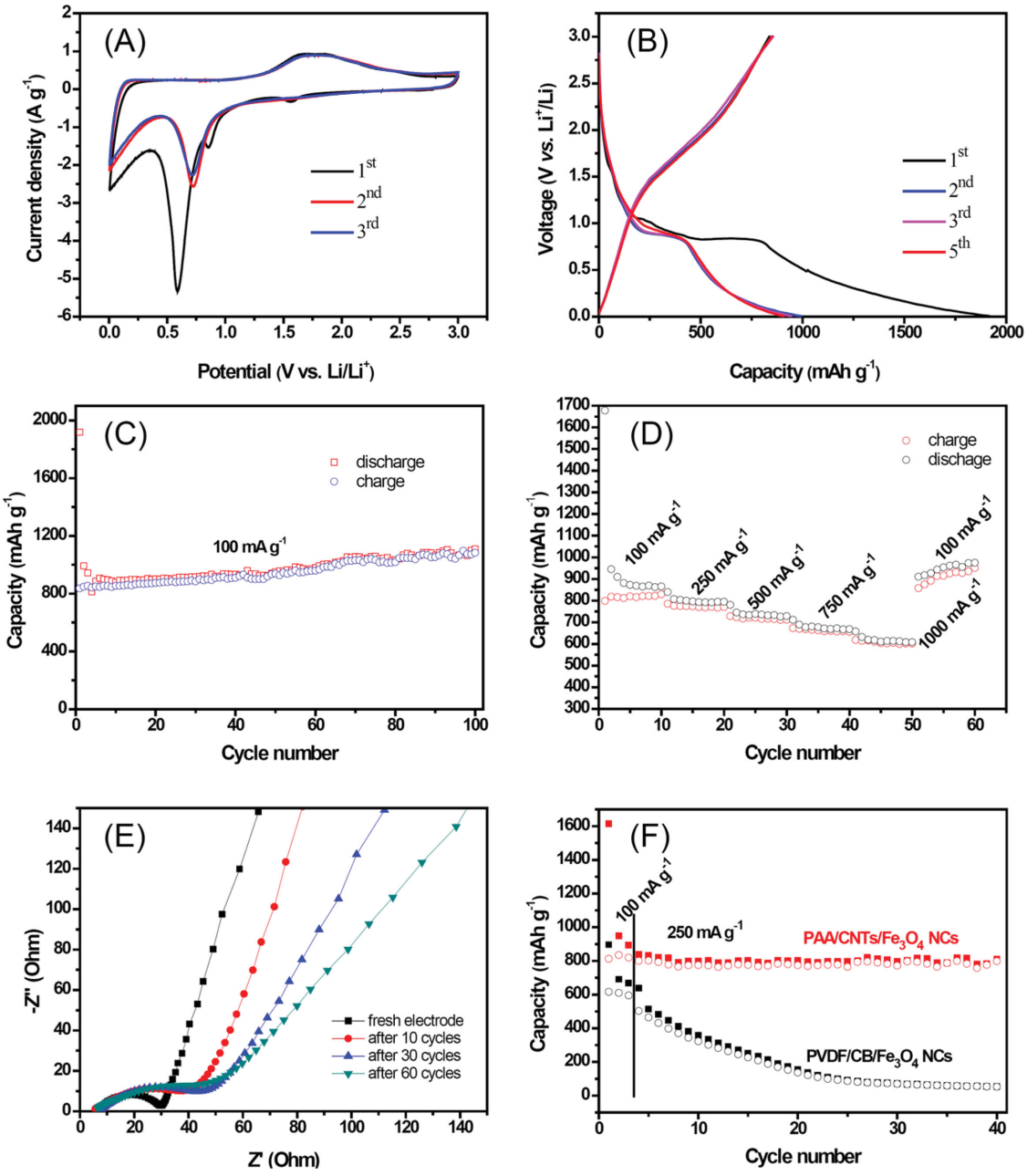

Figure 3. A) CV plots of the CNTs/Fe_3O_4 electrode for the first three cycles at a sweep rate of 0.5 mV s^{-1}. B) Typical galvanostatic charge/discharge curves of the composite electrode at a current density of 100 mA g^{-1}. C) Long-term cycling performance of the electrode at current density of 100 mA g^{-1}. D) Rate performance of the CNTs/Fe_3O_4 electrode at different current densities. E) Nyquist plots of the CNTs/Fe_3O_4 electrode at different cycling status at high-frequency range. F) Comparison of specific capacity versus cycle number for CNTs/Fe_3O_4 electrode and control Fe_3O_4 electrode at 250 mA g^{-1}.

As a control, Fe_3O_4 NCs were mixed with carbon black (CB) and polyvinylidene fluoride (PVDF) by conventional slurry methods. However, such electrodes showed poor stability with rapid capacity fading as seen in Figure 3F. The results indicate that the PAA/CNTs networks do play an important role to buffer the large volume changes and maintain good electrical contacts with active materials during the cycling. Besides the Fe_3O_4 NCs, this method is also applicable to a wide range various materials, independent of size and shape. For example, the rod-like MnO_2 (tetragonal α-MnO_2 phase, Figure S5, Supporting Information), and CNTs can be also assembled into a 3D network using the same approach above, and excellent rate capability and cycling stability are also obtained (Figure S6, Supporting Information). The polymer selection is flexible; in addition to PAA, polymer with similar functional groups such as polyvinyl alcohol (PVA) can also be used to make nanocomposites with high performance (Figure S7, Supporting Information). For example, PVA/CNTs/Fe_3O_4 composite electrodes also showed high capacity and good cycling stability that comparable with PAA/CNTs/Fe_3O_4 electrodes, indicating that our methodology can be generally applied to a broad range of materials.

In summary, we have demonstrated a polymer-assisted assembling strategy to fabricate Li electrodes using the hydrophilic active materials and CNTs. The superior electrode performance is attributed to the strong interaction between each constituent in a porous conductive CNTs network. This study provides a supramolecular chemistry strategy to build complex systems for flexible electrodes applications. The possibility of using different polymers and active oxide nanoparticles opens up the potential of this approach to be applied for a wide range of materials, and perhaps it can be extended to other applications, such as catalysts, solar cells, and chemical sensing.

Experimental Section

Synthesis of Fe_3O_4 NCs and MnO_2 NCs: The Fe_3O_4 nanoparticles were synthesized using the method described in the literature.[39] 1.1 g of $FeCl_2{\cdot}4H_2O$ and 3 g of $FeCl_3{\cdot}6H_2O$ were added into 150 mL of deionized water in a 250 mL round flask, stirred vigorously under a nitrogen atmosphere at 50 °C, and then combined with 12.5 mL of ammonia solution (25%). The reaction solution was cooled down after 30 min reaction, the Fe_3O_4 nanoparticles was collected by filtration, followed by washing with deionized water for three times, and then dried using freeze drying. The synthesis of MnO_2 nanorods was followed the description in ref. [40].

Fabrication of Film Electrodes: A free-standing film electrodes was fabricated by a vacuum filtration method. First, the pristine CNTs producing from a CVD method were purified using an 18% HCl solution and a 20% HF solution alternatively to remove residual catalysts,[12] followed by washing with piranha solutions (4:1, v/v 96% H_2SO_4/30% H_2O_2) at 0 °C for 2 h for better dispersion.[41] The weakly-oxidized CNTs were then dispersed in DMSO to form a 1 mg/mL solution by using a JJ-2 homogenated fluid shearing machine at around 3000 r min^{-1} for 2 h. The above 5 mL of CNTs solution was mixed with 5 mg of polyacrylic acid (PAA, Sigma Aldrich, *Mw*: 4.5×10^5 g mol^{-1}), and 15 mg of Fe_3O_4 NCs in ethanol solution was subsequently added into the above solution. Then, vacuum filtration produces free-standing composite films. The nylon six membrane (Jingteng) was used as a filter with diameter of 50 mm and average pore size of 0.45 μm. The flexible film was punched into discs to get CNTs/Fe_3O_4 electrodes followed by annealing under nitrogen atmosphere for 5 h at 300 °C. Similarly, CNT/MnO_2 electrode (weight ratio, 15:15:70) was prepared in the same way with that of PAA/CNT/Fe_3O_4 electrode. As control, conventional electrodes were made by mixing the Fe_3O_4 NCs with CB and PVDF (HSV 900, from Kynar) at same weight ratio of 3:1:1 with that of CNT/Fe_3O_4 composite and then vacuum dried at 100 °C for 8 h.

Characterization: The morphology and structure of Fe_3O_4/CNTs composites were investigated by transmission electron microscope (TEM, Philips CM120, 120 kV), scanning electron microscope (SEM, FEI Nova 600) and XRD (Rigaku Miniflex II, Cu–Kα radiation). N_2 adsorption/desorption isotherms were determined using a Micromeritics ASAP 2020 analyzer. TGA was conducted on a TGA SDT Q600 instrument at a ramping rate of 10 °C min^{-1} in air.

For electrochemical test, the film electrodes as working electrode were assembled into 2032-type coin cells in an argon-filled glove box, metallic Li as the counter/reference electrode, and glass fiber papers from Whatman as the separators. The electrolyte solution was 1.0 M $LiPF_6$ in ethylene carbonate/diethyl carbonate (1:1 by volume) with additional vinylene carbonate (2% by volume). CV and EIS measurement were performed by Solartron 1287/1260 electrochemical interface. The galvanostatic charge/discharge measurements were carried out at various current densities over a voltage range of 0.005–3 V (vs. Li/Li^+) using LAND CT2000 battery tester.

Supporting Information

Supporting Information is available from the Wiley Online Library or from the author.

Acknowledgements

Y.C. and Z.C. contributed equally to this work. This work was partially supported by the National Natural Science Foundation for Distinguished Young Scholar of China (No. 50925312), the Program for Changjiang Scholars and Innovation Research Team in University (T2011079, IRT1221), and the China Scholarship Council. This research work was supported as part of the Molecularly Engineered Energy Materials, an Energy Frontier Research Center funded by the U.S. Department of Energy, Office of Science, Office of the Basic Energy Sciences under award DE-SC001342 (Z.C., Y. L.).

Received: July 18, 2014
Revised: September 13, 2014
Published online:

[1] Z. Wang, L. Zhou, X. W. Lou, *Adv. Mater.* **2012**, *24*, 1903.
[2] Y. Chen, H. Xia, L. Lu, J. Xue, *J. Mater. Chem.* **2012**, *22*, 5006.
[3] T. Muraliganth, A. Vadivel Murugan, A. Manthiram, *Chem. Commun.* **2009**, 7360.
[4] P. G. Bruce, B. Scrosati, J. M. Tarascon, *Angew. Chem. Int. Ed.* **2008**, *47*, 2930.
[5] H. B. Wu, J. S. Chen, H. H. Hng, X. Wen Lou, *Nanoscale* **2012**, *4*, 2526.
[6] W. Shi, X. Rui, J. Zhu, Q. Yan, *J. Phys. Chem. C* **2012**, *116*, 26685.
[7] R. Liu, J. Duay, S. B. Lee, *Chem. Commun.* **2011**, *47*, 1384.
[8] M. Sathiya, A. S. Prakash, K. Ramesha, J. Tarascon, A. K. Shukla, *J. Am. Chem. Soc.* **2011**, *133*, 16291.
[9] M. D. Lima, S. Fang, X. Lepró, C. Lewis, R. Ovalle-Robles, J. Carretero-González, E. Castillo-Martínez, M. E. Kozlov, J. Oh, N. Rawat, C. S. Haines, M. H. Haque, V. Aare, S. Stoughton, A. A. Zakhidov, R. H. Baughman, *Science* **2011**, *331*, 51.
[10] H. Fei, Z. Peng, L. Li, Y. Yang, W. Lu, E. G. Samuel, X. Fan, J. Tour, *Nano Res.* **2014**, *7*, 1.
[11] H. X. Zhang, C. Feng, Y. C. Zhai, K. L. Jiang, Q. Q. Li, S. S. Fan, *Adv. Mater.* **2009**, *21*, 2299.
[12] X. Jia, C. Yan, Z. Chen, R. Wang, Q. Zhang, L. Guo, F. Wei, Y. Lu, *Chem. Commun.* **2011**, *47*, 9669.
[13] Z. Chen, D. Zhang, X. Wang, X. Jia, F. Wei, H. Li, Y. Lu, *Adv. Mater.* **2012**, *24*, 2030.
[14] Z. Chen, Y. Yuan, H. Zhou, X. Wang, Z. Gan, F. Wang, Y. Lu, *Adv. Mater.* **2014**, *26*, 339.
[15] R. Janot, D. Guérard, *Prog. Mater. Sci.* **2005**, *50*, 1.
[16] X. Zhao, C. M. Hayner, H. H. Kung, *J. Mater. Chem.* **2011**, *21*, 17297.
[17] Z. Wang, Z. Wu, N. Bramnik, S. Mitra, *Adv. Mater.* **2014**, *26*, 970.
[18] X. Jia, Z. Chen, A. Suwarnasarn, L. Rice, X. Wang, H. Sohn, Q. Zhang, B. M. Wu, F. Wei, Y. Lu, *Energy Environ. Sci.* **2012**, *5*, 6845.
[19] Y. Wu, Y. Wei, J. Wang, K. Jiang, S. Fan, *Nano Lett.* **2013**, *13*, 818.
[20] M. S. Strano, *Nat. Mater.* **2006**, *5*, 433.
[21] M. T. Byrne, Y. K. Gun'ko, *Adv. Mater.* **2010**, *22*, 1672.
[22] H. X. Wu, T. J. Wang, Y. Jin, *Ind. Eng. Chem. Res.* **2007**, *46*, 761.
[23] J. Fresnais, M. Yan, J. Courtois, T. Bostelmann, A. Bée, J. F. Berret, *J. Colloid. Interface Sci.* **2013**, *395*, 24.
[24] J. Fresnais, J. F. Berret, B. Frka-Petesic, O. Sandre, R. Perzynski, *Adv. Mater.* **2008**, *20*, 3877.
[25] P. L. Taberna, S. Mitra, P. Poizot, P. Simon, J. M. Tarascon, *Nat. Mater.* **2006**, *5*, 567.
[26] I. Kovalenko, B. Zdyrko, A. Magasinski, B. Hertzberg, Z. Milicev, R. Burtovyy, I. Luzinov, G. Yushin, *Science* **2011**, *334*, 75.

[27] N. Yabuuchi, K. Shimomura, Y. Shimbe, T. Ozeki, J. Y. Son, H. Oji, Y. Katayama, T. Miura, S. Komaba, *Adv. Energy Mater.* **2011**, *1*, 759.
[28] A. Magasinski, B. Zdyrko, I. Kovalenko, B. Hertzberg, R. Burtovyy, C. F. Huebner, T. F. Fuller, I. Luzinov, G. Yushin, *ACS Appl. Mater. Interfaces* **2010**, *2*, 3004.
[29] B. Koo, H. Kim, Y. Cho, K. T. Lee, N. S. Choi, J. Cho, *Angew. Chem. Int. Ed.* **2012**, *51*, 8762.
[30] Z. Wang, D. Luan, S. Madhavi, Y. Hu, X. W. Lou, *Energy Environ. Sci.* **2012***5*, 5252.
[31] X. Jia, Z. Chen, X. Cui, Y. Peng, X. Wang, G. Wang, F. Wei, Y. Lu, *ACS Nano* **2012**, *6*, 9911.
[32] Y. He, L. Huang, J. S. Cai, X. M. Zheng, S. G. Sun, *Electrochim. Acta* **2010**, *55*, 1140.
[33] G. Zhou, D. W. Wang, F. Li, L. Zhang, N. Li, Z. S. Wu, L. Wen, G. Q. Lu, H. M. Cheng, *Chem. Mater.* **2010**, *22*, 5306.
[34] S. K. Behera, *Chem. Commun.* **2011**, *47*, 10371.
[35] E. Frackowiak, S. Gautier, H. Gaucher, S. Bonnamy, F. Beguin, *Carbon* **1999**, *37*, 61.
[36] S. H. Ng, J. Wang, Z. P. Guo, J. Chen, G. X. Wang, H. K. Liu, *Electrochim. Acta* **2005**, *51*, 23.
[37] S. Laruelle, S. Grugeon, P. Poizot, M. Dollé, L. Dupont, J. M. Tarascon, *J. Electrochem. Soc.* **2002**, *149*, A627.
[38] Y. Kou, Y. Xu, Z. Guo, D. Jiang, *Angew. Chem. Int. Ed.* **2011**, *50*, 8753.
[39] X. Chen, L. Li, X. Sun, Y. Liu, B. Luo, C. Wang, Y. Bao, H. Xu, H. Peng, *Angew. Chem. Int. Ed.* **2011**, *50*, 5486.
[40] B. Li, G. Rong, Y. Xie, L. Huang, C. Feng, *Inorg. Chem.* **2006**, *45*, 6404.
[41] K. J. Ziegler, Z. Gu, H. Peng, E. L. Flor, R. H. Hauge, R. E. Smalley, *J. Am. Chem. Soc.* **2005**, *127*, 1541.